Journal of Power Sources 210 (2012) 47–53

Contents lists available at SciVerse ScienceDirect

Journal of Power Sources

journal homepage: www.elsevier.com/locate/jpowsour

A simple solvothermal route to synthesize graphene-modified $LiFePO_4$ cathode for high power lithium ion batteries

Yin Zhang, Wenchao Wang, Penghui Li, Yanbao Fu, Xiaohua Ma*

Department of Materials Science, Fudan University, Shanghai 200433, People's Republic of China

ARTICLE INFO

Article history:
Received 3 February 2012
Received in revised form 29 February 2012
Accepted 2 March 2012
Available online 7 March 2012

Keywords:
Graphene
Lithium iron phosphate
Lithium ion batteries
Solvothermal synthesis

ABSTRACT

To improve the rate performance and cycling stability of $LiFePO_4$, graphene-modified $LiFePO_4$ composite has been developed as Li-ion battery cathode material. The composite is successfully prepared *via* a novel solvothermal route. C-$LiFePO_4$/graphene, with structure of C-$LiFePO_4$ nanoparticles embedded in graphene matrix, exhibits excellent electrochemical properties, including superior high-rate capability and favorable charge–discharge cycle performance under relative high current density. The size of $LiFePO_4$ nanoparticles can be controlled below 30 nm with good reproducibility through this route and due to the synergism of thin carbon film and graphene matrix, the dual coatings exert a significant impact on the electronic conductivity. This novel composite presents excellent electrochemical properties: with reversible capacity of 90 mAh g^{-1} at 10C and 42 mAh g^{-1} at 40C achieved.

1. Introduction

Following the pioneering work by Padhi et al. in 1997 [1], $LiFePO_4$, with an olivine structure, is considered to be a promising positive electrode material due to its high theoretical capacity (170 mAh g^{-1}), low cost, environment benignity, cycling stability and high safety [2,3], all of which has naturally led to a fast development in the application of plug-in hybrid vehicles [4]. The most common methods to prepare $LiFePO_4$ are solid-state reaction, coprecipitation, hydrothermal, solvothermal, sol–gel and microwave reaction [5,6]. Nonetheless, $LiFePO_4$ has some intrinsic shortcomings, including poor electronic conductivity and limited lithium ion diffusion coefficiency, which result in less impressive performance at high rates [7,8]. Many efforts have been made to overcome these limitations, during which carbon coating is the most common method, which is widely applied and systemically studied [9,10]. However, the rate-performance enhancement of such electrode materials is still limited, for thin carbon layer arising from low carbon content can hardly form an effective continuous carbon network that bridges the particles to enhance the electrical contact, and if the volume of carbon is increased to form a continuous network, the energy density of the cell will be decreased [10,11]. Chen et al. showed that the presence of carbon, even a little amount, would cause a significant tap density decrease [12]. Hu et al. found when using a novel conductive RuO_2 filled the gap of coated carbon, the $LiFePO_4$ charge and discharge cycling performance had significantly improved. But RuO_2 is expensive and the experiment is complicated, so it's not practical for application [15]. Fedorkova et al. proposed a new way to modify $LiFePO_4$ with PPy/PEG, but these strategies had only given a modest enhancement of performance. So the cycling stability at high rate performance still remains a challenge [13].

Since the discovery of graphene with single graphite layer structure [14], it has attracted a lot of attention for various reasons such as superior mechanical properties and electrical conductivity [15,16]. Graphene-based composites considered as a kind of exciting material that has many potential applications [17], and it may be an ideal way to hybrid $LiFePO_4$ with graphene to form a nano-structured electrode and solve the problem mentioned above [18]. Individual or chemical modified graphene sheets are typically prepared through several techniques including the scotch tape (peel off) method [19], epitaxial growth [20], CVD [21], and chemical reduction of suspensions of graphene oxide [22,23]. However, for the reason of thermodynamic instable structure of graphene, it tends to aggregate in the aqueous solution. Recently Li et al. reported generation of homogeneous aqueous suspension of chemically modified graphene sheets by using dialysis when maintaining pH 10 [24]. Zhou et al. explored a simple hydrothermal route to convert graphite oxide (GO) to stable graphene suspension without any reducing agent, and the thickness of graphene sheets was only 0.81 nm [25].

Recent research had shown that lithium ion conductivity could be improved by considering the size and crystal orientation of $LiFePO_4$ [26]. Although traditional hydrothermal/solvothermal

* Corresponding author. Tel.: +86 2155664024; fax: +86 2155664024.
E-mail address: xhma@fudan.edu.cn (X. Ma).

0378-7753/$ – see front matter © 2012 Elsevier B.V. All rights reserved.
doi:10.1016/j.jpowsour.2012.03.007

synthesis routes have already shown incomparable advantages in synthesizing many other compounds with controlled size and crystal orientation [27], it is still a great challenge to explore an effective route for self-assembly novel nano-$LiFePO_4$ architectures with ideal loading density.

In contrast to other *ex situ* methods reported before [28,29], we designed a simple *in situ* solvothermal route to prepare C-$LiFePO_4$ composite which is embedded in graphene matrix as nanoparticles. The size of $LiFePO_4$ nanoparticles could be controlled below 30 nm with good reproducibility, and the loading efficiency could be also notably enhanced. With the novel structure we can overcome the major disadvantages of lithium ion diffusing limitation for poor electronic conductivity without the induction of new ions so as to provide excellent electrochemical properties.

2. Experimental

2.1. Synthesis of C-$LiFePO_4$/graphene composite

All the chemicals are analytic grade, and used as received. The graphite oxide (GO) was prepared by modified Hummers method [30]. The $LiFePO_4$/graphene nanocomposite was prepared through an *in situ* solvothermal route: typically a mixture of $FeCl_2{\cdot}4H_2O$, LiH_2PO_4 with the molar ratios of 1:1.05 was dissolved in 100 mL ethylene glycol, and 50 μL hydrazine and 50 mg GO were added in after ultrasonic dispersion while stirring constantly for 1 h under nitrogen atmosphere. The resulting homogeneous solution was then transferred into a 150 mL stainless autoclave, and was heated at 250 °C for 8 h. After cooled to ambient temperature, the black participates was obtained by centrifugation, and then washed for several times with distilled water. After drying in the vacuum oven at 60 °C overnight, as-synthesized $LiFePO_4$/graphene was mixed and ground with citric acid, and acetone was added to make a uniform slurry mixture, here citric acid acted as carbon source and resulted a uniform carbon coating on the $LiFePO_4$ particles. The mixture was annealed at 600 °C for 3 h in an Ar/H_2 atmosphere ($Ar:H_2$ = 95:5) in order to carbonize citric acid and perfect the defective graphene sheets, as well as to increase the crystallinity of the C-$LiFePO_4$/graphene samples.

2.2. Structure and electrochemical characterization

X-ray powder diffraction (XRPD) was obtained by a Rigaku D/max-γB X-ray diffractometer with Cu Kα irradiation (λ = 1.5418 Å) at 40 kV and 100 mA.

Inductive coupled plasma emission spectrometer (ICP-AES) was recorded by a Hitachi P-4010 Inductive coupled plasma emission spectrometer, the range of λ was 165–1000 nm, and RSD < 5%.

Raman spectroscopy was recorded by a Dilor LabRam-1B Raman microscope (Dilor, France), operating at a resolution of 1 cm^{-1}.

X-ray photoelectron spectroscopy (XPS) was obtained by a PHI 5000C ESCA System with Al/Mg irradiation at 14 kV and 300 W in the range of 0–1200 eV (constant pass energy 50 eV).

The scanning electron microscopy (SEM) analysis had been performed using a JEOL-JSM-8701F field emission SEM (JEOL, Japan) and operated at 3 kV. Transmission electron microscope (TEM) observation was acquired using a Hitachi H600 transmission electron microscope (Hitachi, Japan). High-resolution transmission electron microscopy (HRTEM) images were obtained by a Philips CM200/FEG field emission transmission electron microscope operated at accelerating voltage of 200 kV.

Atomic force microscopy (AFM) analysis was carried out in Shimadzu SPM-9500J3 scanning probe microscope (Shimadzu, Japan), with dynamic contact mode to investigate the surface morphology of the sample.

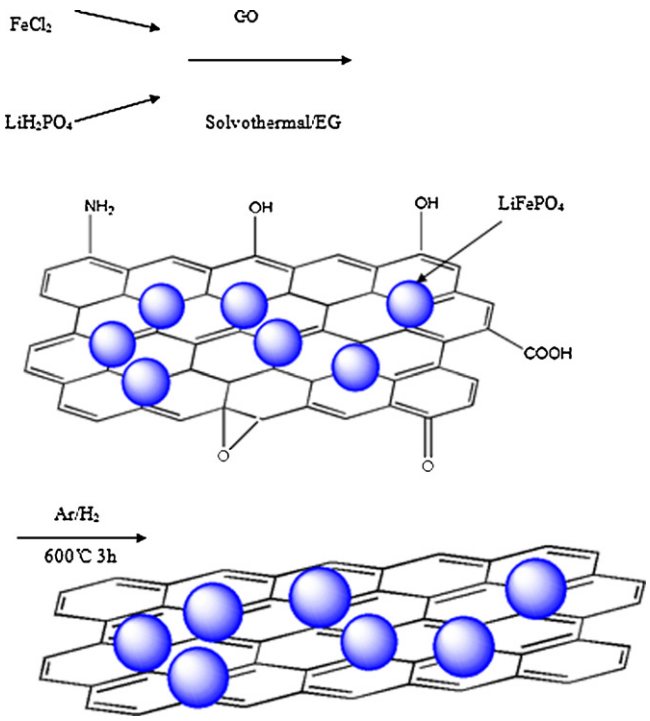

Scheme 1. Preparation procedures of $LiFePO_4$/graphene by *in situ* solvothermal route.

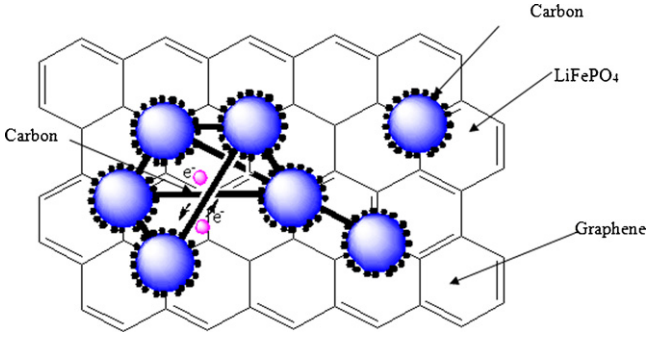

Fig. 1. The simulated structure of C-$LiFePO_4$/graphene.

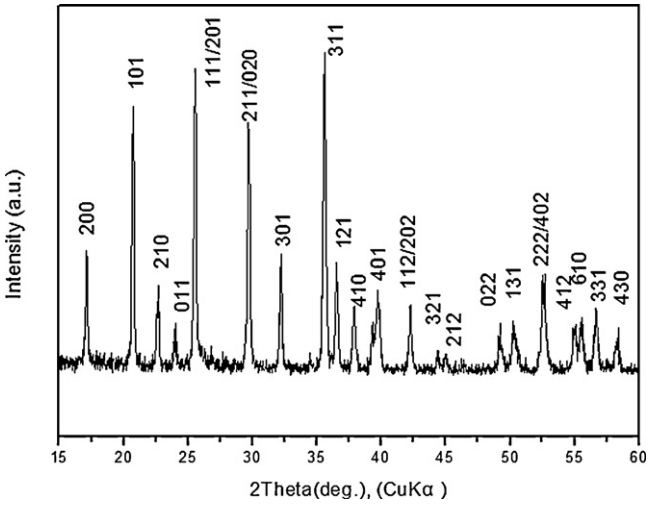

Fig. 2. XRPD pattern of the C-$LiFePO_4$/graphene composite.

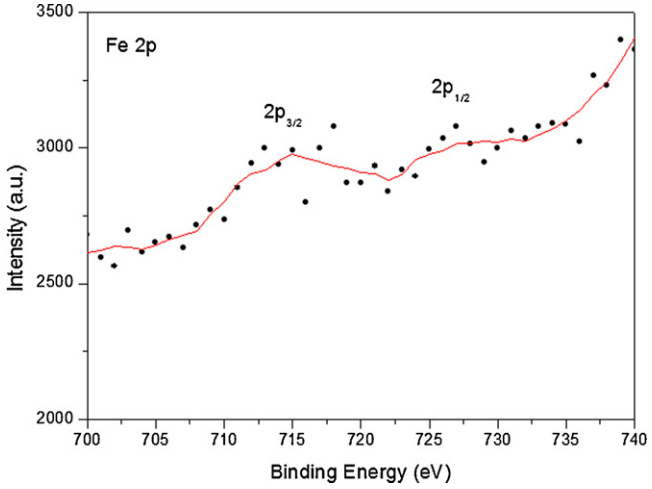

Fig. 3. XPS spectra of C-$LiFePO_4$/graphene composite.

For electrochemical characterization, a composite electrode was prepared as follows: a mixture of 80 wt% C-$LiFePO_4$/graphene composite, 12 wt% carbon black and 8 wt% polyvinylidinedifluoride (PVDF) was dissolved in N-methylpyrrolidone (NMP), stirred vigorous for 3–6 h. Then the slurry was coated onto an etched aluminum foil current collector with a blade. The electrode was dried for 12 h at 120 °C in a vacuum oven, followed by pressing compactly with a roller press machine. Lithium metal foil was used as the anode and a Celgard 2400 was used as a separator. The electrolyte was composited of 1 M $LiPF_6$ in ethylene carbonate (EC):dimethyl carbonate (DMC):diethyl carbonate (DEC) (1:1:1, v/v/v). The CR2016 coin type cells were assembled in an Argon-filled glove box (MBraun Lab Master 130, Germany). Similarly the electrochemical impedance spectrum (EIS) measurement was synthesized using the same coin cells except that the mixture was consisted of 92 wt% C-$LiFePO_4$/graphene composite and 8 wt% PVDF with no carbon black added.

The galvanostatic charge/discharge cycles were performed at varied C-rates (charge and discharge using the same C-rate) with cutoff voltage of 2.5 and 4.2 V *vs.* Li/Li^+, using a LAND-CT2001A cycle life tester (Wuhan Jinnuo Electronics Co., Ltd., China), cyclic voltammetry (CV) and electrochemical impedance spectrum (EIS) measurements were conducted using Solartron SI 1260 Gain Phase Analyzer/SI 1287 Electrochemical Interface (Solartron, UK), the scanning rate was 0.1 mV s^{-1}. All the electrochemical tests were carried under 25 °C.

3. Results and discussion

Scheme 1 shows the formation process of $LiFePO_4$/graphene, $LiFePO_4$ nanoparticles were prepared by the controlled solvothermal synthesis method, while graphene nanosheets were reduced in the presence of hydrazine *via in situ* reaction. In our experiment, ethylene glycol (EG) was employed as reaction medium to make sure that the mass transportation rates of different ions species can match each other [31]. Because the viscosity of EG (η = 21 mPa s, 20 °C) is much higher than that of water ($\eta = 1.0087 \times 10^{-3}$ mPa s, 20 °C). The diffusive rates of ions would be reduced significantly in this medium. Consequently, the mobility rates of different ions species (Li, Fe) could match each other in this high-viscosity mixture medium. Moreover, EG acted as a soft template for facilitating the self-assembly of *in situ* grown nanoparticles through forming hydrogen bonds. Hydrogen bonding between the hydroxyl groups in EG allows it to exist in the long chain form, and individual GO platelets were also interlinked *via* a non-uniform network of hydrogen bonds. Cations in the reaction mixture may be trapped in the

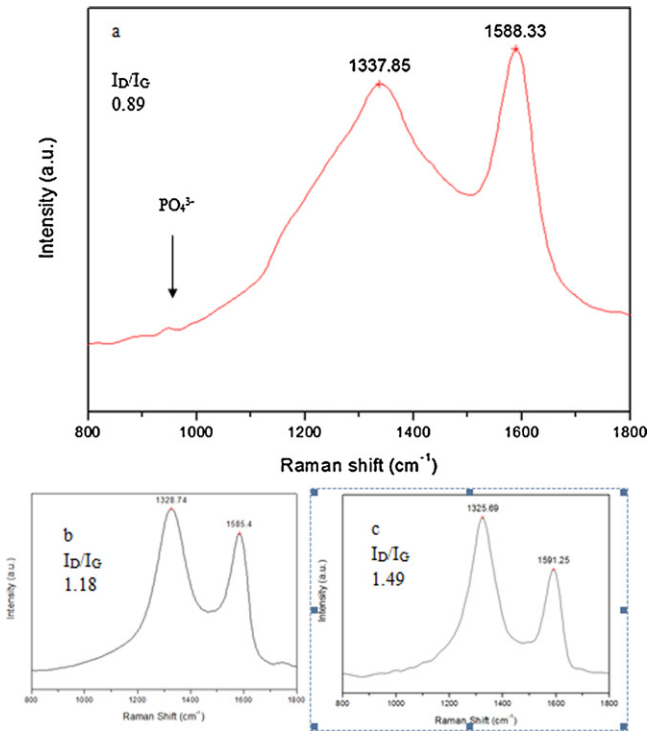

Fig. 4. Raman spectra of (a) C-$LiFePO_4$/graphene, (b) GO, and (c) hydrazine-reduced GO.

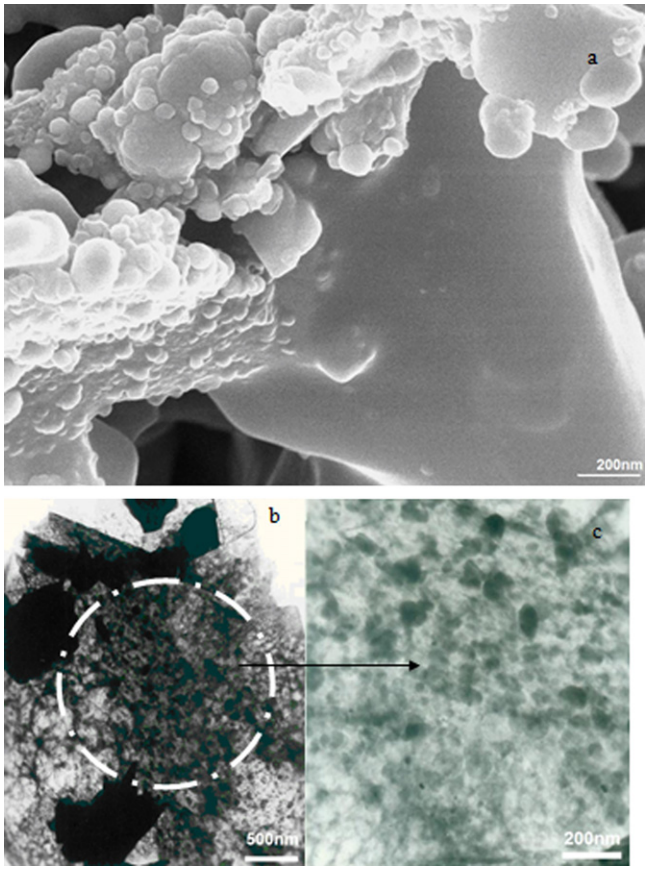

Fig. 5. (a) SEM image of C-$LiFePO_4$/graphene, (b) TEM image of C-$LiFePO_4$/graphene, and (c) the magnified image of (b).

network of hydrogen bonds which assist nucleation and control the crystal growth of $LiFePO_4$ [26,32]. It is also worth mentioning that EG can enhance the combination between $LiFePO_4$ particles and graphene nanosheets compared to that in the water system [33].

Herein, it was worth mentioning that using Ar/H_2 in the heat treatment could perfect the defective graphene nanosheets. Note that the graphene was obtained through chemical reduction from GO, so it still contained a few residual oxygen atoms [34,35]. The presence of sp^3 sites disrupted the flow of charge carriers through sp^2 clusters and would lower the Li-ion diffusion coefficient.

Fig. 1 exhibits the simulated structure of the synthesized C-$LiFePO_4$/graphene sample. We can deduce that the carbon film is thin and heterogeneous, and there is partial effective carbon network that bridges the particles, which can be proved by transmission electron microscopy (TEM) results later.

The weight ratio of Fe in $LiFePO_4$/graphene and C-$LiFePO_4$/graphene was determined by ICP-AES, which was 30.8% for $LiFePO_4$/graphene and 26.6% for C-$LiFePO_4$/graphene, so the content of graphene was 13.1 wt% and carbon was 11.8 wt%.

The X-ray powder diffraction (XRPD) pattern of C-$LiFePO_4$/graphene is shown in Fig. 2. The XRPD pattern clearly exhibits single phase formation of $LiFePO_4$; all the peaks in the XRPD are indexed on the basis of an orthorhombic space group (JCPDS Card No: 40-1499), demonstrating that $LiFePO_4$ is highly crystallized without any detectable impurity phases.

The X-ray photoelectron spectroscopy (XPS) spectrum of Fe $2p_{3/2}$ (Fig. 3) shows a binding energy (BE) of 715 eV which matches with the BE of Fe^{2+} in $LiFePO_4$. Due to the multiple splitting of energy levels Fe ion gives rise to satellite peaks around 727 eV.

Raman spectroscopy was used to characterized the hydrazine reduced graphite oxide (GO) and C-$LiFePO_4$/graphene, for comparison, the Raman spectrum of GO is also shown (Fig. 4). The Raman spectrum of C-$LiFePO_4$/graphene displays two typical and broad bands at 1338 cm^{-1} of D band and 1588 cm^{-1} of G band (Fig. 4a). The G band is usually assigned to the E_{2g} photon of C sp^2 atoms, while the D band is a breathing mode of κ-point photons of A_{1g} symmetry. A prominent D band is an indication of disorder-allowed zone-edge modes of graphite, along with amorphous carbon species [36,37]. The intensity ratio (I_D/I_G) of D band to G band of the GO was about 1.18, while for hydrazine-reduced GO, the I_D/I_G has increased to 1.49 after the treatment, which is due to the presence of unrepaired defects that remained after the removal of oxygen moieties. It is instructive to note that the I_D/I_G for C-$LiFePO_4$/graphene is

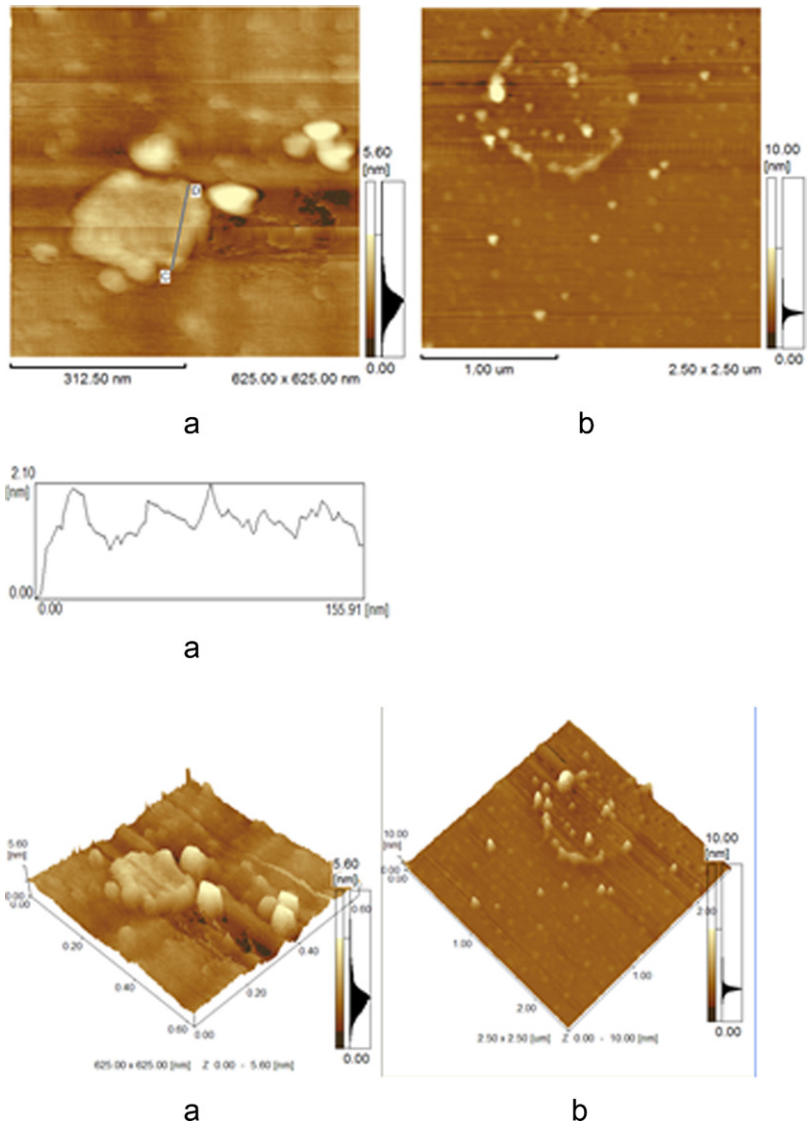

Fig. 6. AFM observation and analysis of graphene (a) and C-$LiFePO_4$/graphene (b).

0.89, which is lowest. Therefore, we can conclude that thermal treatment with Ar/H_2 can perfect the defective graphene nanosheets so that allow the modification of the electronic properties of graphene readily.

The structure of morphology of C-$LiFePO_4$/graphene is characterized by scanning electron microscope (SEM) and transmission electron microscope (TEM) (Fig. 5).

The SEM image of Fig. 5a presents the aggregated C-$LiFePO_4$ nanoparticles with 30–250 nm in diameter embedded on graphene sheets, the agglomeration in varying degrees is due to the large surface area and consequently the high surface energy. Furthermore, the long solvothermal reaction time coupled with high annealing temperature is likely responsible for the agglomeration of nanoparticles.

As observed in Fig. 5b and c, lots of C-$LiFePO_4$ nanoparticles are embedded in the graphene sheet with favorable dispersion. And it is conspicuous that part of C-$LiFePO_4$ nanoparticles is connected by "carbon bridges", which complies with the simulated structure mentioned above.

The morphological features of graphene and C-$LiFePO_4$/graphene were characterized by AFM (Fig. 6). It reveals that graphene sheets with lateral dimension of 200–2000 nm, and heights in the range of 1–4 nm. As can be seen from Fig. 3b, the surface of graphene is covered with C-$LiFePO_4$ nanoparticles. By controlling the solvothermal conditions, the deposit can be attached to the graphene well, though there are still some unattached $LiFePO_4$ particles.

The high resolution transmission electron microscopy (HRTEM) image (Fig. 7) exhibits detailed features in nanometer domain. The clear lattice fringes reveal the single crystallinity, and the width of 6.6 Å of neighboring lattice fringes correspond to the (2 0 1) plane of $LiFePO_4$.

Fig. 8 shows the cyclic voltammetry (CV) curves of carbon coated $LiFePO_4$ and C-$LiFePO_4$/graphene at a scan rate of 0.1 mV s^{-1} after activation for 3 cycles. The symmetry of the oxidation and reduction peaks in the CV plots confirmed the better reversibility of lithium extraction/insertion reactions in C-$LiFePO_4$/graphene compared with C-$LiFePO_4$. The CV peak currents, I_p, used to evaluate the

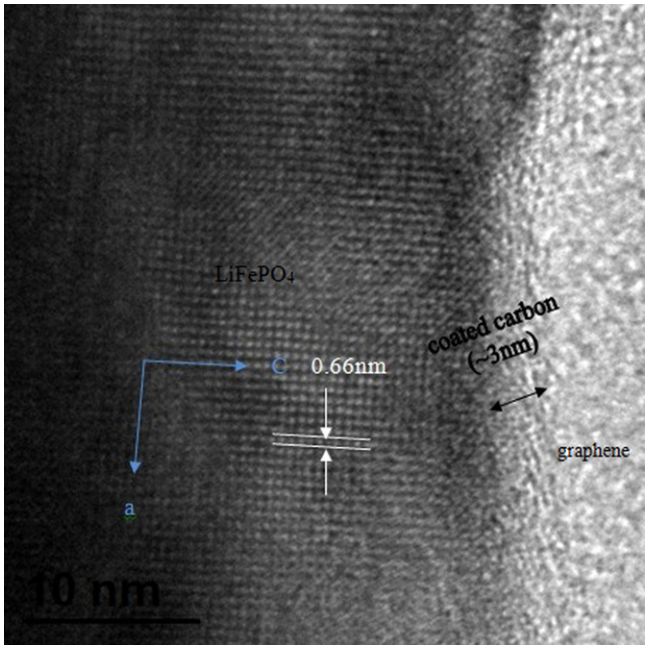

Fig. 7. HRTEM images of C-$LiFePO_4$/graphene.

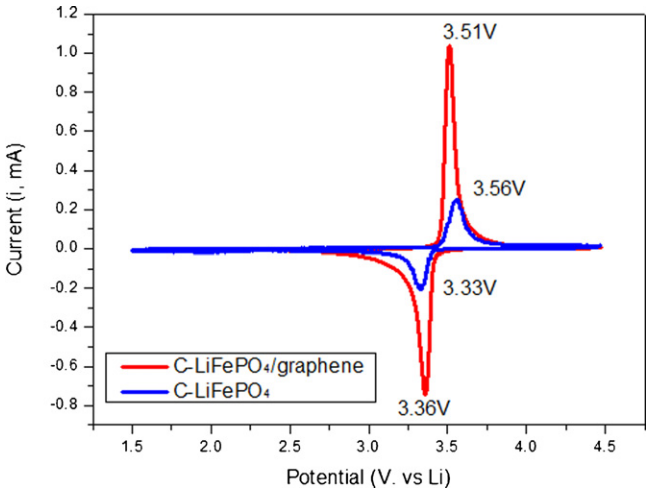

Fig. 8. Cyclic voltammograms of C-$LiFePO_4$/grapahene and C-$LiFePO_4$.

Li^+ diffusion coefficient D, according to the Randles–Sevcik equation [38]:

$$I_p = 2.69 \times 10^5 ACD^{1/2} n^{3/2} v^{1/2}$$

where I_p is the peak currents (A), A is the electrode area (cm^2), C is the shuttle concentration (mol cm^{-3}), n is the number of electrons involved in the redox process ($n = 1$ for Fe^{2+}/Fe^{3+} redox pair), and v is the potential scan rate (0.1 mV s^{-1} in this experiment).

It can be seen form Fig. 8 that C-$LiFePO_4$/graphene shows much sharper current peaks than C-$LiFePO_4$, because graphene is large, thin and has good electrical conductivity, compared to coated carbon, so both Li^+ ion and electron can be available at the same spot on the surface of C-$LiFePO_4$/graphene particles, with the supply of electrons by extremely conductive graphene, which leads to higher diffusion coefficient of Li-ions.

Typical charge/discharge curves of samples at the cycling rate of 0.1C were displayed in Fig. 9. The voltage difference between the flat charge and discharge plateaus (ΔV) was related to the polarization of the cell system. The polarization was caused by slow lithium diffusion in the active material and increases in the resistance of the electrolyte when the charging–discharging rate increased. After graphene nanosheets incorporating, ΔV was reduced from 85 mV to 54 mV, with a irreversible capacity of about

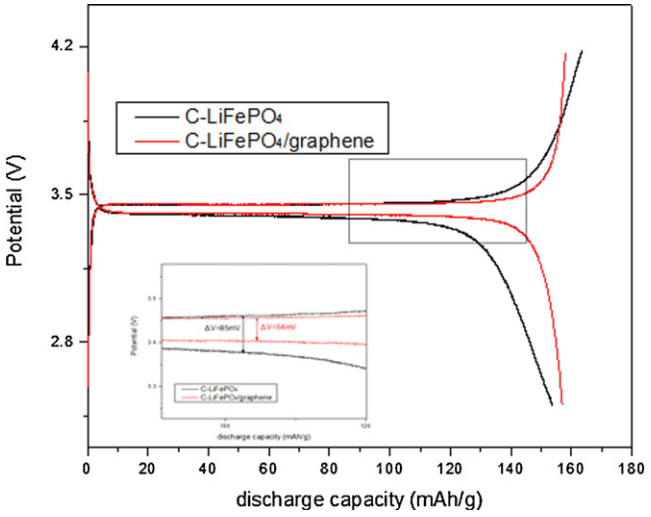

Fig. 9. The typical charge/discharge profiles of C-$LiFePO_4$/graphene and C-$LiFePO_4$ at a current rate of 0.1C, the insets show the flat regions magnified.

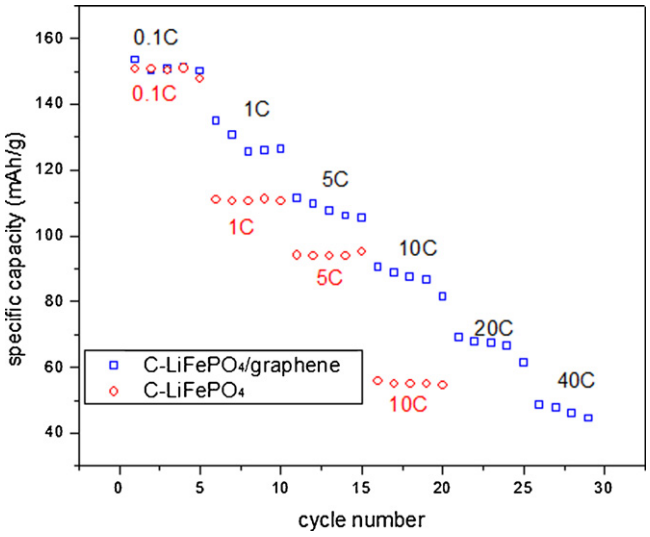

Fig. 10. Discharge cycling performances of C-$LiFePO_4$/graphene and C-$LiFePO_4$ samples at different discharging rates from 0.1C to 40C at room temperature.

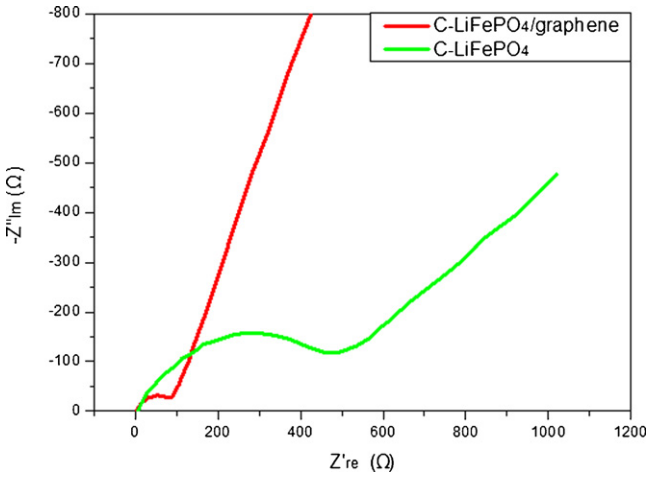

Fig. 11. Impedance spectra of C-$LiFePO_4$ and C-$LiFePO_4$/graphene.

5 mAh g^{-1}, indicating that the kinetics of the $LiFePO_4$ was indeed improved after graphene incorporating. The reason was graphene presented surprisingly robust transport properties and behaved like a metal with almost high constant mobility over a large range of temperatures and charge densities.

The more remarkable advantage of this nano-hybrid material is the high-rate capability. Fig. 10 shows the specific discharge capacities *vs.* cycle number at various current rates for C-$LiFePO_4$ and C-$LiFePO_4$/graphene. At a given low rate (0.1C), both samples delivered a capacity of ~160 mAh g^{-1}. However, at higher discharge rates, in contrast, the cell prepared with C-$LiFePO_4$/graphene scored clearly better than the other one. The reversible capacity of C-$LiFePO_4$/graphene could be achieved at 90 mAh g^{-1}, even at 20C and 40C, a reversible capacity of 72.7 mAh g^{-1} and 42 mAh g^{-1} could be achieved, whereas the value for graphene-free sample was negligible.

The tremendously improved rate capability and excellent cycling stability can be ascribed to the favorable lithium ion transport and the 3D electron transfer highways built from interweaved graphene nanosheets. The 3D network of graphene offers a considerable benefit over conventional carbon coating in terms of enhancing the electron conductivity within the secondary particles. It can be delineated continuous graphene layers which wrap homogeneously around the surface of $LiFePO_4$ nanoparticles are served as a fast path for electron migration during charge/discharge processes.

In order to gain a deep understanding of the influence on the charge transfer, the electrochemical impedance spectra (EIS) was carried out (Fig. 11). The EIS data were collected with a two electrode coin cell (without the additive of carbon black) after activation. Both profiles exhibit a semicircle in the high frequency region and a straight line in the low-frequency region. The numerical value of the diameter of the semicircle on the Z_{real} axis is approximately equal to the charge transfer resistance (R_{ct}) [39]. The straight line is attributed to the diffusion of the lithium ions into the bulk of the electrode material or so-called Warburg diffusion. The intercept impedance on the Z_{real} axis represents the ohmic resistance, which consists of the resistance of the electrolyte and electrode. It is found the R_{ct} of C-$LiFePO_4$ only approximately 100 Ω, revealing a remarkable decrease in charge transfer resistance after addition of graphene, which is related to the improvement in electronic conductivity provided by graphene.

4. Conclusion

We had succeeded in preparing a kind of graphene-modified $LiFePO_4$ cathode material through a solvothermal route, exhibiting favorable electrochemical properties. A key to its realization is: we assembled $LiFePO_4$ nanoparticles and graphene sheets in a manner that $LiFePO_4$ was embedded in graphene matrix as nanoparticles, and the graphene matrix served as mixed conducting nano-network, enabling optimal mixed electronic-ionic transport. The relatively simple availability of GO nanosheets offered potential for application in high-power electrical sources. Moreover, the preparation strategy we developed was easily transferable to other cathode or anode materials with low conductivity to produce series of high performance electrode materials.

References

[1] A.K. Padhi, K.S. Nanjundaswamy, J.B. Goodenough, J. Electrochem. Soc. 144 (1997) 1188–1194.
[2] P.S. Herle, B. Ellis, N. Coombs, L.F. Nazar, Nat. Mater. 3 (2004) 147–152.
[3] M. Yonemura, A. Yamada, Y. Takei, N. Sonoyama, R. Kanno, J. Electrochem. Soc. 151 (2004) A1352–A1356.
[4] P. Reale, S. Panero, B. Scrosati, J. Garche, M. Wohlfahrt-Mehrens, M. Wachtler, J. Electrochem. Soc. 151 (2004) A2138–A2142.
[5] K.S. Park, K.T. Kang, S.B. Lee, G.Y. Kim, Y.J. Park, H.G. Kim, Mater. Res. Bull. 39 (2004) 1803–1810.
[6] T. Muraliganth, A.V. Murugan, A. Manthiram, J. Mater. Chem. 18 (2008) 5661–5668.
[7] S.Y. Chung, J.T. Bloking, Y.M. Chiang, Nat. Mater. 1 (2002) 123–128.
[8] C.C. Li, Y.H. Wang, T.Y. Yang, J. Electrochem. Soc. 158 (2011) A828–A834.
[9] R. Dominko, J.M. Goupil, M. Bele, M. Gaberscek, M. Remskar, D. Hanzel, J. Jamnik, J. Electrochem. Soc. 152 (2005) A858–A863.
[10] J.D. Wilcox, M.M. Doeff, M. Marcinek, R. Kostecki, J. Electrochem. Soc. 154 (2007) A389–A395.
[11] R. Dominko, M. Bele, M. Gaberscek, M. Remskar, D. Hanzel, S. Pejovnik, J. Jamnik, J. Electrochem. Soc. 152 (2005) A607–A610.
[12] Z.H. Chen, J.R. Dahn, J. Electrochem. Soc. 149 (2002) A1184–A1189.
[13] A. Fedorkova, R. Orinakova, A. Orinak, I. Talian, A. Heile, H.D. Wiemhofer, D. Kaniansky, H.F. Arlinghaus, J. Power Sources 195 (2010) 3907–3912.
[14] K.S. Novoselov, A.K. Geim, S.V. Morozov, D. Jiang, Y. Zhang, S.V. Dubonos, I.V. Grigorieva, A.A. Firsov, Science 306 (2004) 666–669.
[15] J.S. Wu, W. Pisula, K. Mullen, Chem. Rev. 107 (2007) 718–747.
[16] S. Dubin, S. Gilje, K. Wang, V.C. Tung, K. Cha, A.S. Hall, J. Farrar, R. Varshneya, Y. Yang, R.B. Kaner, ACS Nano 4 (2010) 3845–3852.
[17] D. Du, J. Liu, X.Y. Zhang, X.L. Cui, Y.H. Lin, J. Mater. Chem. 21 (2011) 8032–8037.
[18] A.K. Geim, Science 324 (2009) 1530–1534.
[19] K.S. Novoselov, D. Jiang, F. Schedin, T.J. Booth, V.V. Khotkevich, S.V. Morozov, A.K. Geim, Proc. Natl. Acad. Sci. U.S.A. 102 (2005) 10451–10453.
[20] C. Berger, Z.M. Song, X.B. Li, X.S. Wu, N. Brown, C. Naud, D. Mayou, T.B. Li, J. Hass, A.N. Marchenkov, E.H. Conrad, P.N. First, W.A. de Heer, Science 312 (2006) 1191–1196.
[21] Z.P. Chen, W.C. Ren, L.B. Gao, B.L. Liu, S.F. Pei, H.M. Cheng, Nat. Mater. 10 (2011) 424–428.
[22] S. Stankovich, D.A. Dikin, G.H.B. Dommett, K.M. Kohlhaas, E.J. Zimney, E.A. Stach, R.D. Piner, S.T. Nguyen, R.S. Ruoff, Nature 442 (2006) 282–286.

[23] Y.X. Xu, K.X. Sheng, C. Li, G.Q. Shi, J. Mater. Chem. 21 (2011) 7376–7380.
[24] D. Li, M.B. Muller, S. Gilje, R.B. Kaner, G.G. Wallace, Nat. Nanotechnol. 3 (2008) 101–105.
[25] Y. Zhou, Q.L. Bao, L.A.L. Tang, Y.L. Zhong, K.P. Loh, Chem. Mater. 21 (2009) 2950–2956.
[26] K. Saravanan, M.V. Reddy, P. Balaya, H. Gong, B.V.R. Chowdari, J.J. Vittal, J. Mater. Chem. 19 (2009) 605–610.
[27] C.A.J. Fisher, M.S. Islam, J. Mater. Chem. 18 (2008) 1209–1215.
[28] X.F. Zhou, F. Wang, Y.M. Zhu, Z.P. Liu, J. Mater. Chem. 21 (2011) 3353–3358.
[29] Y. Ding, Y. Jiang, F. Xu, J. Yin, H. Ren, Q. Zhuo, Z. Long, P. Zhang, Electrochem. Commun. 12 (2010) 10–13.
[30] W.S. Hummers, R.E. Offeman, J. Am. Chem. Soc. 80 (1958) 1339.
[31] F. Teng, S. Santhanagopalan, R. Lemmens, X.B. Geng, P. Patel, D.D. Meng, Solid State Sci. 12 (2010) 952–955.
[32] N.V. Medhekar, A. Ramasubramaniam, R.S. Ruoff, V.B. Shenoy, ACS Nano 4 (2010) 2300–2306.
[33] J.L. Wu, X.P. Shen, L. Jiang, K. Wang, K.M. Chen, Appl. Surf. Sci. 256 (2010) 2826–2830.
[34] H.A. Becerril, J. Mao, Z. Liu, R.M. Stoltenberg, Z. Bao, Y. Chen, ACS Nano 2 (2008) 463–470.
[35] C. Mattevi, G. Eda, S. Agnoli, S. Miller, K.A. Mkhoyan, O. Celik, D. Mostrogiovanni, G. Granozzi, E. Garfunkel, M. Chhowalla, Adv. Funct. Mater. 19 (2009) 2577–2583.
[36] A.C. Ferrari, J.C. Meyer, V. Scardaci, C. Casiraghi, M. Lazzeri, F. Mauri, S. Piscanec, D. Jiang, K.S. Novoselov, S. Roth, A.K. Geim, Phys. Rev. Lett. 97 (2006).
[37] A.C. Ferrari, J. Robertson, Phys. Rev. B 61 (2000) 14095–14107.
[38] Y.D. Cho, G.T.K. Fey, H.M. Kao, J. Power Sources 189 (2009) 256–262.
[39] H. Liu, Q. Cao, L. Fu, C. Li, Y. Wu, H. Wu, Electrochem. Commun. 8 (2006) 1553–1557.